Cerâmica. 2024, v.70:e WYWG7941 http://dx.doi.org/10.1590/WYWG7941
ORIGINAL ARTICLE

Structural, physical, and mechanical properties of Al_2O_3-NbC composite obtained by hot pressing and spark plasma sintering

Paulo H. Chibério[1], Hugo P. A. Alves[2]*, Rubens Alves Junior[3], João M. Dantas Neto[1], Wilson Acchar[1,4]
[1]Postgraduate Program in Materials Science and Engineering,
Federal University of Rio Grande do Norte, 59078-970, Natal, RN, Brazil
[2] Postgraduate Program in Materials Science and Engineering,
Federal University of Paraiba, 58051-900, João Pessoa, PB, Brazil
[3]Postgraduate Program in Materials Science and Engineering,
Federal University of Campina Grande, 58429-900, Campina Grande, PB, Brazil
[4]Department of Physics, Federal University of Rio Grande do Norte, 59078-970, Natal, RN, Brazil

Abstract

In this study, we produced, through hot pressing (HP) and spark plasma sintering (SPS) techniques, Al_2O_3-NbC composites for applications in machining processes. We report an experimental investigation of sintered composites' structural, thermal, morphological, physical, and mechanical properties. The results confirm that the Al_2O_3-NbC composite sintered by both techniques presents a heterogeneous microstructure with distinct grain sizes and irregular geometries. Another stimulating factor is the increase of 25.86% in Vickers hardness, 14.89% in Young's modulus, and 16.52% in mechanical strength of the composite sintered by SPS about the composite sintered by HP. Thus, our results can be used to address material properties targeting the needs of specific technological applications.
Keywords: alumina, niobium carbide, hot pressing, spark plasma sintering, mechanical properties

INTRODUCTION

WC-Co cermet-based cutting tools have dominated the manufacturing market in recent years [1–4]. However, these materials exhibit some problems related to the high production cost and the raw materials' toxicity [5]. A solution to this problem is the development of alumina-carbide composite materials due to better fracture toughness, high hardness, and better abrasion strength when compared to traditional WC-Co tools. Duan; Wang; Xing [6] show that multiscale textures effectively improve the cutting performance of Al_2O_3-TiC ceramic tools. Yin et al. [7] indicate that the microwave-sintered Al_2O_3-SiC ceramic tool satisfies the requirements in high-speed machining applications. Zhao et al. [8] note satisfactory results in the growth of TaC whiskers in an Al_2O_3 ceramic matrix for cutting tools. Jung and Lee [9] reveal that the Al_2O_3-B_4C composite has higher microhardness and toughness than the monolithic Al_2O_3, making it suitable for cutting tool performance.

Among these carbides, we highlight niobium carbide (NbC) because it has interesting physical and mechanical properties when incorporated into a ceramic matrix [10, 11]. However, its greater refractoriness hinders the composite's densification, allowing for a more significant formation of porosity and, consequently, a decrease in hardness [12]. In this sense, the development of dense composites for applications in machining becomes essential.

We can highlight the hot pressing (HP) and plasma spark sintering (SPS) techniques from this perspective [13, 14]. These techniques become suitable for obtaining materials with high densification and ultrafine microstructures, improving mechanical and structural properties [15, 16].

Therefore, this work aims to produce, through the hot pressing and spark plasma sintering technique, dense Al_2O_3-NbC composites for applications in machining processes. Consequently, we will analyze the efficiency of sintering techniques and their influence on structural, thermal, morphological, physical, and mechanical properties.

EXPERIMENTAL PROCEDURE

Alumina (α-Al_2O_3, purity > 99.99 %, the average particle size of 150 nm, the density of 3.98 g/cm^3; Taimei Chemicals, Tokyo, Japan) and 30 wt.% niobium carbide (NbC, purity > 99.99 %, the average particle size of 2.5 μm, the density of 7.82 g/cm^3; Herman Starck, Berlin, Germany) were used as ceramic powders. The proportion of niobium carbide used in this work was chosen due to its excellent mechanical and structural responses. Ceramic powders were dispersed in isopropyl alcohol for 5 h in a planetary milling process. Then, the ceramic compound was dried in an oven at 60 ºC for 4 h.

After homogenization, equal amounts of ceramic powders (20 g) sieved using 200 mesh grids (< 74 μm) were placed in a cylindrical graphite matrix with an internal diameter of 30 mm, being fabricated and sintered by hot pressing (Weitai Technol. Develop. Ltd. Co., Shenyang, China) and spark

* *eng.hugoplinio@gmail.com*
https://orcid.org/0000-0003-3408-943X

plasma sintering (SPS, Dr. Sinter SPS 211-LX, Saitama, Japan). In HP sintering, a pressure of 30 MPa in argon flow was used at a final temperature of 1500 ºC for 120 min, with a heating rate of 20 º/min. In SPS sintering, the pressure was 40 MPa at a final temperature of 1500 °C for 5 min, with a heating rate of 65 º/min. The thermocouple and the infrared thermometer were selected to measure the temperature on the matrix's surface. In the end, five samples were prepared for each test, performed posteriorly.

The thermal expansion behavior was performed for Al_2O_3 powder and Al_2O_3-NbC composite, pre-pressed in an 8 mm diameter matrix, using a high-sensitivity DIL 402 C simple push-rod dilatometer (Netzsch) in an argon atmosphere with a heating rate of 5 °/min. The crystallographic characterizations were investigated using an X-ray diffractometer (XRD), model Rigaku Miniflex II, with CuKα radiation obtained at 30 kV (with filament current at 15 mA), measuring range of 20º < 2θ < 80º, scanning with an angular step of 0.02º, and counting time by step of 5º/min. Rietveld refinement of the XRD patterns was performed, thus providing information on the crystalline phase content, crystallite size, lattice parameters, and quality factors. Fourier transform infrared spectroscopy (FTIR) was performed in PerkinElmer equipment, model spectrum 65, with a resolution of 4 cm^{-1}. The morphological images were observed through a scanning electron microscope with a field emission source (SEM-FEG), model Zeiss Auriga 40. The relative density of the composite was obtained by the ratio between the actual and theoretical density, where the actual density was measured using Archimedes' rule, and the theoretical density was tested using the simple rule of mixtures. Vickers hardness measurements (VH, Zwick 3212, Zwick) were calculated from the lengths of the cracks and the diagonals produced by the indentation method on polished surfaces, using a load of 4.9N for 15 seconds. The Vickers hardness value was then calculated using equation (A).

$$VH = \frac{F}{A} = 1.8544 \frac{D}{d^2} \qquad (A)$$

where, VH = Vickers Hardness; F = applied force (N); A = Area of print produced; d = length of the diagonals (mm). Young's modulus was calculated from the point of longitudinal and transverse ultrasonic velocities. The mechanical strength at room temperature was measured using a universal testing machine (Zwick-Roell, 2.5kN) in three-point bending tests at a constant crosshead speed of 0.5 mm/min. As for the 3-point bending test, it is necessary to know the cross-sectional area of the samples. The average widths were calculated, obtained at 7.114 mm, and the average for the thicknesses of 4.534 mm. The span (Ls) was 20 mm. For these tests, five specimens were tested for each sample.

RESULTS AND DISCUSSION

Figure 1 shows the dilatometric curves of the Al_2O_3 powder and the Al_2O_3-NbC composite. We observed that both curves present similar behavior, suggesting that incorporating NbC does not alter the sintering behavior of Al_2O_3. Al_2O_3 powder

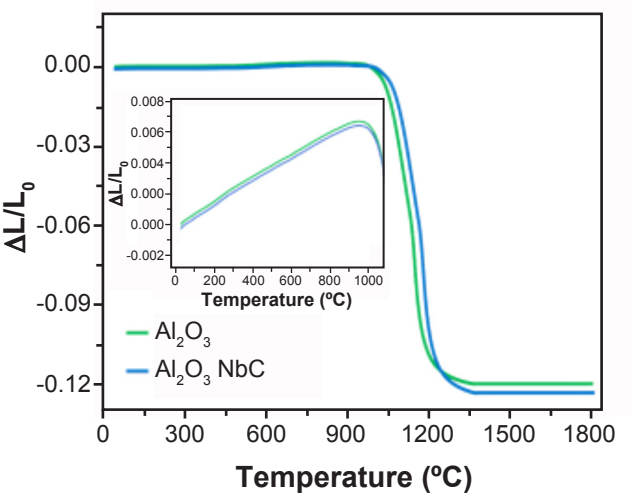

Figure 1: Dilatometric curves of Al_2O_3 powder and Al_2O_3-NbC composite.

and Al_2O_3-NbC composite exhibit a thermal expansion of approximately 0.67% up to 1000 °C. Then, a 12% shrinkage occurs between 1040 ºC and 1350 ºC, indicating the beginning of sintering [17–19].

The refined XRD patterns of the ceramic powders (Al_2O_3 and NbC) and the Al_2O_3-NbC composite sintered by HP and SPS are shown in Figures 2a, b, c, and d. The diffraction peaks are indexed considering the cards ICSD-51687 for α- Al_2O_3 with hexagonal symmetry and space group P6 and ICSD-

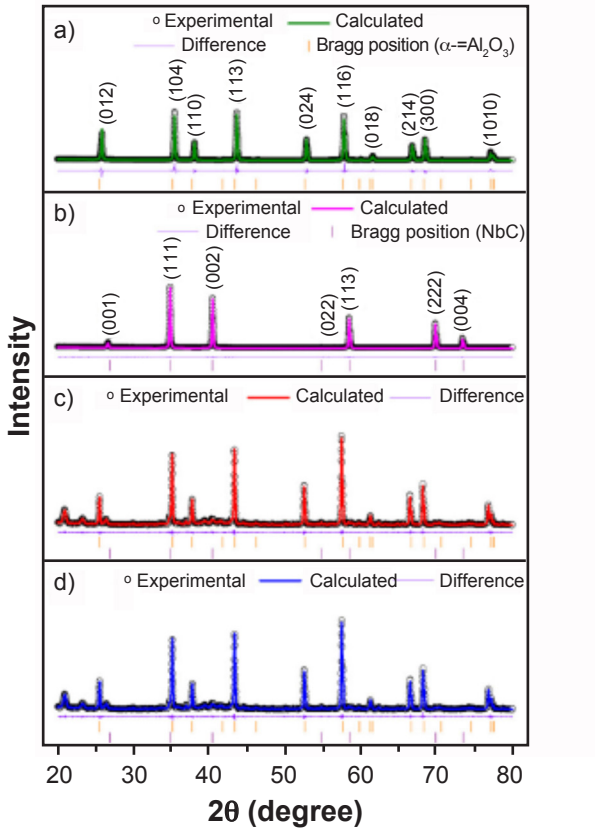

Figure 2: XRD patterns of (a) Al_2O_3 and (b) NbC ceramic powders and Al_2O_3-NbC composite sintered by (c) HP and (d) SPS.

Table I: Parameters obtained from the Rietveld refinement.

Sample	Symmetry	Space Group	wt (%)	Latt. Par. (Å)	Size (nm)	R_{wp} I χ^2
Al_2O_3	Hexagonal	P6	100	a = b = 5.0289(8) c = 12.7762(3)	100.01	16.08 I 1.12
NbC	Cubic	P23	100	a = b = c = 4.4744(8)	99.97	16.03 I 1.09
HP	Hexagonal (α-Al_2O_3)	P6	69.87	a = b = 5.0277(8) c = 12.7767(3)	71.85	16.48 I 1.22
	Cubic (NbC)	P23	30.13	a = b = c = 4.4721(8)	61.20	
SPS	Hexagonal (α-Al_2O_3)	P6	69.94	a = b = 5.0279(8) c = 12.7758(3)	63.96	16.33 I 1.34
	Cubic (NbC)	P23	30.06	a = b = c = 4.4757(8)	54.40	

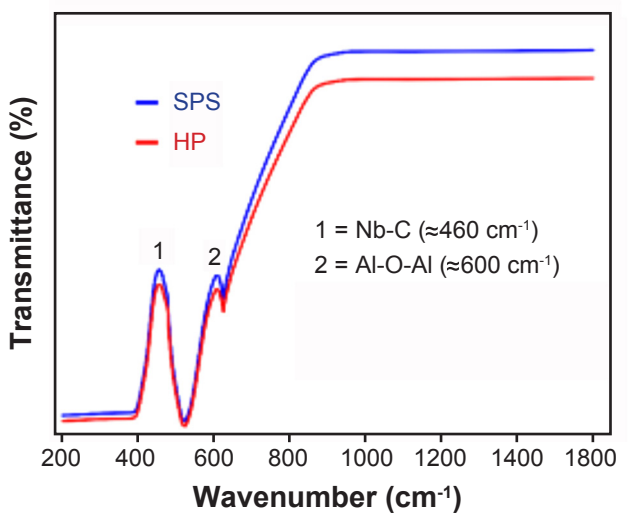

Figure 3: FTIR absorption spectra of the Al_2O_3-NbC composite sintered by HP and SPS.

43373 for NbC with cubic symmetry and space group P23. Through Rietveld analysis, the Al_2O_3 sample has the lattice parameters a = b = 5.0289(8) Å and c = 12.7762(3) Å, with a crystallite size of 100.01 nm. The NbC sample shows the lattice parameters a = b = c = 4.4744(8) Å, with a crystallite size of 99.97 nm. The quality of Rietveld refinement for these samples is confirmed by the parameters R_{wp} and χ^2. The Rietveld refinement quality factors are 16.08 and 1.12 for Al_2O_3, while for NbC, these values are 16.03 and 1.09, respectively. For the Al_2O_3-NbC composite sintered by HP and SPS, we verified the presence of the α-Al_2O_3 and NbC phases, in which the Rietveld refinement quality factors are 16.48 and 1.22 for the composite sintered by HP and 16.33 and 1.34 for the sintered composite by SPS. The lattice parameters obtained for the composite sintered by HP are a = b = 5.0277(8) Å and c = 12.7767(3) Å for α-Al_2O_3 and a = b = c = 4.4721(8) Å for NbC, while for the composite sintered by SPS is a = b = 5.0279(8) Å and c = 12.7758(3) Å for α-Al_2O_3 and a = b = c = 4.4757(8) Å for NbC. The crystallite size of Al_2O_3 and NbC, respectively, is 71.85 nm and 61.20 nm for the HP-sintered composite and 63.96 nm and 54.40 nm for the SPS-sintered composite. We observed an approximately 11% decrease in crystallite size for the SPS-sintered composite. This fact is related to the high heating rate used during the sintering process, as reported by Alecrim et al. [20]. Table 1 displays the parameters obtained from the Rietveld refinement discussed previously. We noticed a good agreement between the values calculated via refinement and the experimental values via XRD.

To investigate the oxidation potential of NbC, we

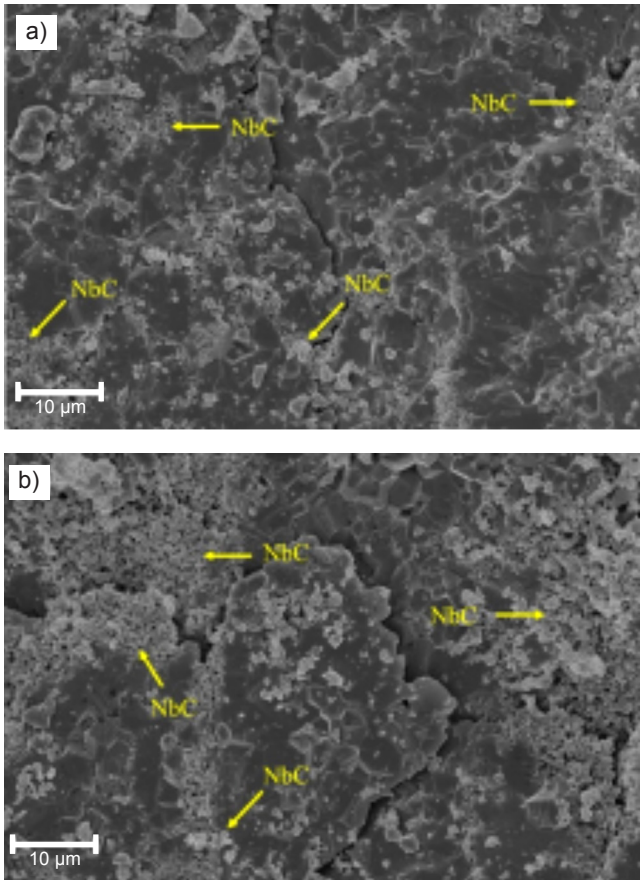

Figure 4: SEM image of the composite sintered by (a) HP and (b) SPS

Table II: Relative density, Vickers hardness, Young's modulus, and mechanical strength of the Al_2O_3-NbC composite sintered by HP and SPS.

Sintering	Relative density (%)	Vickers hardness (GPa)	Young's Modulus (GPa)	Mechanical strength (MPa)
HP	97.42 ± 1.29	20.45 ± 1.79	285.90 ± 32.11	234.94 ± 20.94
SPS	98.23 ± 1.12	27.58 ± 2.07	335.94 ± 29.55	281.42 ± 23.23

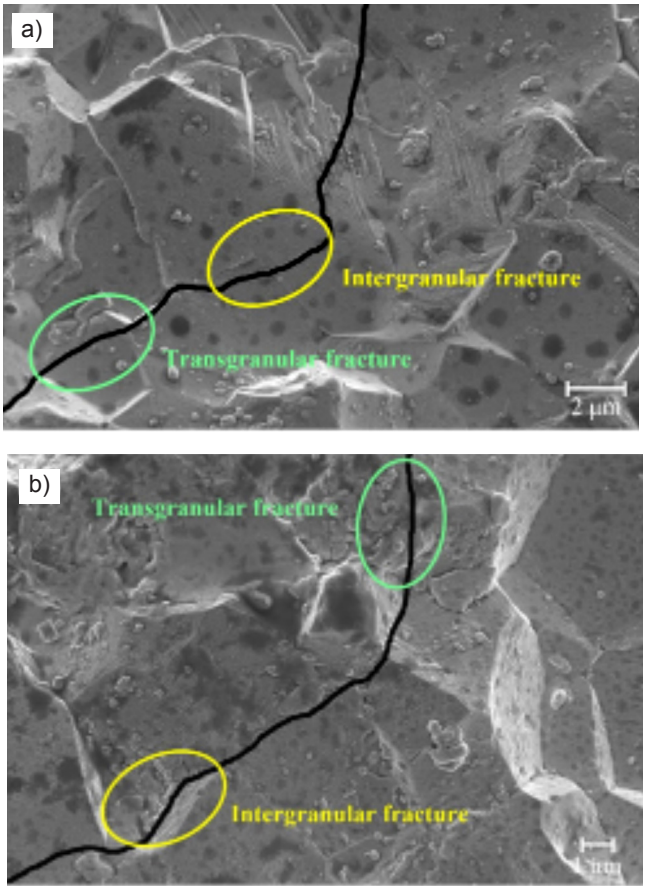

Figure 5: SEM image showing a mixed mode of transgranular fracture and intergranular fracture for composite sintered by (a) HP and (b) SPS.

performed FTIR spectroscopy on the Al_2O_3-NbC composite sintered by HP and SPS, as seen in Figure 3. Both curves exhibit two bands, the first at 460 cm^{-1} characteristics of a low-frequency band of the Nb-C group [21] and the second at 600 cm^{-1} attributed to the Al-O-Al bending mode [22]. Therefore, we noticed the absence of NbC oxidation, corroborating the XRD results. A similar effect is found in work done by Acchar et al. [23].

Figures 4a, b present the sintered composites' structural characterization through SEM images. The microstructure of the composite sintered by HP is like that sintered by SPS. We verified small grains of NbC heterogeneously dispersed in the Al_2O_3 matrix, which agrees with the literature [14, 24]. Furthermore, we noticed morphologies with distinct grain sizes and irregular geometries. Salem et al. [25] attributed this to uniaxial pressure applied during sintering.

Table 2 compares the physical and mechanical responses of composites sintered by HP and SPS. According to the results, the relative density, Vickers hardness, Young's modulus, and mechanical strength of composites sintered by SPS are superior to those of HP. Nečina and Pabst [26] associated this with a higher heating rate and shorter sintering time of composites sintered by SPS, which produces lower grain growth. We found satisfactory results compared with the literature [27–29], strengthening our findings.

Through the SEM image, Figures 5a, b, we verified a mixed mode of transgranular fracture and intergranular fracture for the composites sintered by HP and SPS. Zaki et al. [30] noticed that the second-phase grains incorporated in the ceramic matrix contribute to the mixed mode of transgranular fracture and intergranular fracture. Other researchers have revealed similar results [31–34].

CONCLUSION

We verified that Al_2O_3-NbC composites are successfully prepared by hot pressing and spark plasma sintering techniques. These techniques allow for heterogeneous microstructures with distinct grain sizes and irregular geometries. The maximum relative density values, Vickers hardness, Young's modulus, and mechanical strength are 98.23%, 27.58 GPa, 335.94 GPa, and 281.42 MPa, respectively, obtained by the SPS technique. Thus, our results pave the way to improve the physical and mechanical performance of the Al_2O_3-NbC composite, targeting current and future technological applications.

ACKNOWLEDGMENT

The authors acknowledge financial support from the Brazilian agencies CAPES and CNPq.

REFERENCES

[1] Lay S, Loubradou M, Schubert W. Structural Analysis on Planar Defects Formed in WC Platelets in Ti□Doped WC–Co. J. Am. Ceram. Soc. 2006;**89**:3229–3234. doi:10.1111/j.1551-2916.2006.01218.x.

[2] Johansson SAE, Wahnström G. A computational study of thin cubic carbide films in WC/Co interfaces. Acta Mater. 2011;**59**:171–181. doi:10.1016/j.actamat.2010.09.021.

[3] Zhang H, Xiong J, Guo Z, Yang T, Liu J, Hua T. Microstructure, mechanical properties, and cutting performances of WC-Co cemented carbides with Ru

additions. Ceram. Int. 2021;**47**:26050–26062. doi:10.1016/j.ceramint.2021.06.011.
[4] Yang J, Roa JJ, Schwind M, Odén M, Johansson-Jõesaar MP, Llanes L. Grinding-induced metallurgical alterations in the binder phase of WC-Co cemented carbides. Mater. Charact. 2017;**134**:302–310. doi:10.1016/j.matchar.2017.11.004.
[5] Woydt M, Mohrbacher H, Vleugels J, Huang S. Niobium carbide for wear protection – tailoring its properties by processing and stoichiometry. Met. Powder Rep. 2016;**71**:265–272. doi:10.1016/j.mprp.2015.12.010.
[6] Duan R, Wang G, Xing Y. Investigation of novel multiscale textures for the enhancement of the cutting performance of Al2O3/TiC ceramic cutting tools. Ceram. Int. 2022;**48**:3554–3563. doi:10.1016/j.ceramint.2021.10.134.
[7] Yin Z, Yan S, Ye J, Zhu Z, Yuan J. Cutting performance of microwave-sintered sub-crystal Al2O3/SiC ceramic tool in dry cutting of hardened steel. Ceram. Int. 2019;**45**:16113–16120. doi:10.1016/j.ceramint.2019.05.128.
[8] Zhao G, Huang C, Liu H, Xu L, Chong X, Zou B, Zhu H. A study on in situ growth of TaC whiskers in Al2O3 matrix powder for ceramic cutting tools. Mater. Res. Bull. 2012;**47**:2027–2031. doi:10.1016/j.materresbull.2012.04.001.
[9] Jung CH, Lee SJ. Machining of hot pressed alumina–boron carbide composite cutting tool. Int. J. Refract. Met. Hard Mater. 2005;**23**:171–173. doi:10.1016/j.ijrmhm.2005.02.001.
[10] Acchar W, Cairo CA, Segadães AM. TEM study of a hot-pressed Al2O3-NbC composite material. Mater. Res. 2005;**8**:109–112. doi:10.1590/s1516-14392005000100019.
[11] Arantes VL, Genova LM, Guimarães P, Fortulan CA, Vleugels J. Influence of NbC Content on the Wear Resistance of Alumina/Niobium Carbide Tools. Mater. Res. 2021;**24**:20200552. doi:10.1590/1980-5373-mr-2020-0552.
[12] Tang Q, Gong J. Effect of porosity on the microhardness testing of brittle ceramics: A case study on the system of NiO–ZrO2. Ceram. Int. 2013;**39**:8751–8759. doi:10.1016/j.ceramint.2013.04.061.
[13] Schmitt-Radloff U, Kern F, Gadow R. Wire-electrical discharge machinable alumina zirconia niobium carbide composites – Influence of NbC content. J. Eur. Ceram. Soc. 2017;**37**:4861–4867. doi:10.1016/j.jeurceramsoc.2017.07.014.
[14] Pallone EMJ, Trombini V, Botta WJ, Tomasi R. Synthesis of Al2O3–NbC by reactive milling and production of nanocomposites. J. Mater. Process. Technol. 2003;**143-144**:185–190. doi:10.1016/s0924-0136(03)00411-4.
[15] Zhang Z, Liu Y, Liu H. Mechanical properties and microstructure of spark plasma sintered Al2O3-SiCw-Si3N4 composite ceramic tool materials. Ceram. Int. 2022;**48**:5527–5534. doi:10.1016/j.ceramint.2021.11.097.
[16] Güler O, Varol T, Alver Ü, Kaya G, Yıldız F. Microstructure and wear characterization of Al2O3 reinforced silver coated copper matrix composites by electroless plating and hot pressing methods. Mater. Today Commun. 2021;**27**:102205. doi:10.1016/j.mtcomm.2021.102205.
[17] Acchar W, Cairo CAA, Chiberio P. Nano-structured alumina reinforced with NbC. Compos. Struct. 2019;**225**:111109. doi:10.1016/j.compstruct.2019.111109.
[18] Azevêdo HVSB, Raimundo RA, Silva DDS, Morais LMF, Costa FA, Macedo DA, Cavalcante DGL, Gomes UU. Effect of High-Energy Milling and Sintering Temperature on the Properties of Al2O3-WC-Co Composites. J. Mater. Eng. Perform. 2021;**30**:1504–1512. doi:10.1007/s11665-020-05423-3.
[19] Ojaimi CL, Ferreira JA, Chinelatto AL, Salem REP, Chinelatto ASA, Pallone EMJA. Microstructure and mechanical properties of Al2O3/ZrO2 composites by two-step sintering. Int. J. Appl. Ceram. Technol. 2020;**17**:1619–1628. doi:10.1111/ijac.13518.
[20] Alecrim L, Ferreira J, Salvador MD, Borrell A, Pallone E. Wear behavior of conventional and spark plasma sintered Al2O3-NbC nanocomposites. Int. J. Appl. Ceram. Technol. 2018;**15**:418–425. doi:10.1111/ijac.12800.
[21] Shubert VA, Lewis SP. Size-dependence of infrared spectra in niobium carbide nanocrystals. Int. J. Mod. Phys. C. 2012;**23**:1240001. doi:10.1142/s0129183112400013.
[22] Sarkar D, Mohapatra D, Ray S, Bhattacharyya S, Adak S, Mitra N. Synthesis and characterization of sol-gel derived ZrO2 doped Al2O3 nanopowder. Ceram. Int. 2007;**33**:1275–1282. doi:10.1016/j.ceramint.2006.05.002.
[23] Acchar W, da Camara CRF, Cairo CAA, Filgueira M. Mechanical performance of alumina reinforced with NbC, TiC, and WC. Mater. Res. 2012;**15**:821–824. doi:10.1590/s1516-14392012005000120.
[24] Alecrim LRR, Ferreira JA, Gutiérrez-González CF, Salvador MD, Borrell A, Pallone EMJA. Sliding wear behavior of Al2O3-NbC composites obtained by conventional and nonconventional techniques. Tribol. Int. 2017;**110**:216–221. doi:10.1016/j.triboint.2017.02.028.
[25] Salem REP, Monteiro FR, Gutiérrez-González CF, Borrell A, Salvador MD, Chinelatto ASA, Chinelatto AL, Ferreira JA, Pallone EMJA. Effect of Al2O3-NbC nanopowder incorporation on the mechanical properties of 3Y-TZP/Al2O3-NbC nanocomposites obtained by conventional and spark plasma sintering. Ceram. Int. 2018;**44**:2504–2509. doi:10.1016/j.ceramint.2017.10.235.
[26] Nečina V, Pabst W. Influence of the heating rate on grain size of alumina ceramics prepared via spark plasma sintering (SPS). J. Eur. Ceram. Soc. 2020;**40**:3656–3662. doi:10.1016.j.jeurceramsoc.2020.03.057.
[27] Chai J, Zhu Y, Wang Z, Shen T, Liu Y, Niu L, Li S, Yao C, Cui M, Liu C. Microstructure and mechanical properties of SPS sintered Al2O3–ZrO2 (3Y)–SiC ceramic composites. Mater. Sci. Eng. A. 2020;**781**:139197. doi:10.1016.j.msea.2020.139197.
[28] Klimczyk P, Wyżga P, Cyboroń J, Laszkiewicz-Łukasik J, Podsiadło M, Cygan S, Jaworska L. Phase stability and mechanical properties of Al2O3-cBN composites prepared via spark plasma sintering. Diam. Relat. Mater. 2020;**104**:107762. doi:10.1016.j.diamond.2020.107762.
[29] Pourmohammadie Vafa N, Ghassemi Kakroudi M, Shahedi Asl M. Role of h-BN content on microstructure

and mechanical properties of hot-pressed ZrB2–SiC composites. Ceram. Int. 2020;**46**:21533–21541. doi:10.1016.j.ceramint.2020.05.255.
[30] Zaki ZI, Al-qahtani M, Alotaibi SH, El-Sadek MH, Ahmed H, Ahmed YMZ. Combustion synthesis of NbC/ZrO2 composites: Influence of Cr additives on the microstructure and mechanical properties. Int. J. Appl. Ceram. Technol. 2021;**18**:1502–1509. doi:10.1111.ijac.13796.
[31] Wu Y, He W, Guo H. Improved fracture toughness and multiple toughening mechanisms of NdPO4/NdYbZr2O7 composites. Ceram. Int. 2020;**46**:16612–16619. doi:10.1016.j.ceramint.2020.03.234.
[32] Han J, Wang Y, Liu R, Cao Y. Lanthanum zirconate ceramic toughened by ferroelastic domain switching of LaAlO3. Ceram. Int. 2018;**44**:15954–15958. doi:10.1016.j.ceramint.2018.06.016.
[33] Li C, Ma Y, He J, Guo H. Self-toughening behavior of nano yttria partially stabilized hafnia ceramics. Ceram. Int. 2019;**45**:21467–21474.doi:10.1016.j.ceramint.2019.07.137.
[34] Cao Y, Li C, Ma Y, Luo H, Yang Y, Guo H. Mechanical properties and thermal conductivities of 3YSZ-toughened fully stabilized HfO2 ceramics. Ceram. Int. 2019;**45**:12851–12859. doi:10.1016.j.ceramint.2019.03.208.
(Rec. 03/08/2023, Rev. 20/11/2023, Ac. 30/11/2023)
(AE: R. Salomão)